9. J. O'M. Bockris, Z. Nagy, and A. Damjanovic, *This Journal*, **119**, 285 (1972).
10. B. Aurian-Blajeni and M. Tomkiewicz, *ibid.*, **132**, 1511 (1985).
11. P. Scholl, X. Shan, D. Bonham, and G. A. Prentice, *ibid.*, **138**, 895 (1991).
12. M.-B. Liu, G. M. Cook, and N. P. Yao, *ibid.*, **128**, 1663 (1981).
13. M. C. H. McKubre and D. D. Macdonald, *ibid.*, **128**, 524 (1981).
14. M. Cai and S.-M. Park, *ibid.*, **143**, 2125 (1996).
15. C. Cachet, B. Saidani, and R. Wiart, *ibid.*, **139**, 644 (1992).
16. R. D. Armstrong, *Corros. Sci.*, **11**, 693 (1971).
17. C.-H. Pyun and S.-M. Park, *This Journal*, **133**, 2024 (1986).
18. C. Zhang and S.-M. Park, *ibid.*, **134**, 2966 (1987).
19. C. Zhang and S.-M. Park, *ibid.*, **136**, 3333 (1989).
20. H. Zhang and S.-M. Park, *ibid.*, **141**, 718 (1994).
21. H. Zhang and S.-M. Park, *ibid.*, **141**, 1998 (1994).
22. H. Zhang and S.-M. Park, *ibid.*, **141**, 2422 (1994).
23. B.-S. Kim, T. Piao, S. N. Hoier, and S.-M. Park, *Corros. Sci.*, **37**, 557 (1995).
24. B. A. Boukamp, *Equivalent Circuit User's Manual*, 2nd ed., University of Twente, Einshede (1989).
25. J. R. Macdonald, *Impedance Spectroscopy*, John Wiley & Sons Inc., New York (1987).
26. C. Gabrielli, *Identification of Electrochemical Processes by Frequency Response Analysis*, Issue 2, Universite P. et M. Curie, Paris (1984).
27. C. H. Mathewson, *Zinc: The Science and Technology of the Metal, Its Alloys and Compounds*, Reinhold Publ. Corp., New York (1959).
28. I. Epelboin, C. Gabrielli, M. Keddam, and H. Takenouti, *Comprehensive Treatise on Electrochemistry*, J. O'M Brockris, B. E. Conway, and E. B. Yeager, Editors, Vol. 4, p. 151, Plenum Press, New York (1981)
29. M. Keddam, J.-F. Lizee, C. Pallotta, and H. J. Takenouti, *This Journal*, **131**, 2016 (1984).
30. A. J. Bard and L. R. Faulkner, *Electrochemical Methods*, Wiley, New York (1980).
31. H. E. Brown, *Zinc Oxide Rediscovered*, The New Jersey Zinc Company, New Jersey (1959).
32. D. Meyerstein and W. A. Mulac, *J. Phys. Chem.*, **72**, 784 (1968).

Electrochemical Behavior of Thin Anodic Oxide Films on Zircaloy-4

Role of the Mobile Defects

R. Salot and F. Lefebvre-Joud

C.E.A. Grenoble DTP/SECC, 38054 Grenoble Cedex 9, France

B. Baroux*

INP Grenoble/LTPCM, 38402 Saint Martin d'Hères, and Centre de Recherches d'Ugine, 73400 Ugine, France

ABSTRACT

The first stages of the electrochemical oxidation of Zircaloy-4 are investigated using simple electrochemical tests and modeling the passive film modifications occurring as a result of contact with the electrolyte. Variations in electrode potential (open-circuit conditions) or current density (potentiodynamic scans) can be simply explained by a high field ($F \sim 10^6$ V/cm) assisted passive film growth. Under open-circuit conditions, this field does not vary with exposure time (in the 2 h to 48 h range). The minimum electric field for the onset of high-field behavior is also evaluated and found smaller than the theoretical value which can be explained by a variation in the concentration of mobile defects throughout the film. Measurements of the electrode potential decay after a potentiodynamic scan confirm this model, allowing interpretation of the film modification as a combination of two separate phenomena: film growth under a high electric field and point defect annihilation.

Introduction

The general context.—Zircaloy-4, which is a zirconium alloy containing Sn, Fe, Cr, and O, is mainly used in the nuclear industry, especially in pressurized water reactors, as fuel cladding material. For safety reasons, the cladding integrity has to be ensured for its entire working life in the reactor core. In such a case, the oxidation rate of Zircaloy in 300°C pressurized water has to be carefully controlled to make sure that the mechanical properties of the cladding are maintained and that the hydrogen uptake by the cladding is not too high.

The general oxidation reaction of Zr alloys in water is written as

$$Zr + H_2O \rightarrow ZrO_2 + H_2$$

The oxidation process is usually described in two steps with a transition between a cubic and a linear oxidation rate.[1-4] The first part of the kinetics is classical; it is the result of the oxygen diffusion through a growing oxide layer.[5-7] It is generally accepted that after the transition, the barrier between the metal and the water consists of an inner dense oxide layer with a constant thickness.[8]

It has been shown that the microstructure of the oxide layer formed at the very beginning of the oxidation process has a clear influence on the subsequent behavior.[9] More precisely, the initial structure of the oxide (in terms of its grain morphology and size, marked preferential orientation, impurity content, and allotropic form of the oxide) are closely linked to the occurrence of the destabilization of the dense inner layer into a porous nonprotective one with a consequent increase in oxidation rate.[5,10,11]

On the other hand, several works have also highlighted the influence of irradiation on the oxidation behavior of Zircaloy-4 or Ti.[12,13] In order to further analyze the mechanisms which are implicated in such conditions, and especially the role played by irradiation defects, we first study the electrochemical behavior of Zircaloy-4 without irradiation, as a reference to be used later for those experiments under irradiation conditions.

In this work, we focus on these first stages of the oxidation process of Zircaloy-4 from an electrochemical standpoint. We first recall the classical electrochemical properties of thin Zircaloy oxide layers. We then intend to model the beginning of uniform oxide growth using the results of

* Electrochemical Society Active Member.

conventional electrochemical experiments performed at room temperature. Special attention is paid to the role of mobile defects within the oxide layer to help explain the observed behavior.

Thin zirconium oxide film features.—In water as in air, zirconium is immediately covered by a protective oxide film. That leads Mankowski *et al.*[14] to classify Zircaloy-4 as a material which passivates spontaneously. This spontaneous passivation is detectable on a current-potential curve by the absence of an activation peak. The gap between the valence and the conduction bands is 5 eV. Consequently, the native film is an n-type semiconductor with a large bandgap.[15] Its thickness is at least 4 to 6 nm, [16] and it can be considered as a thin film.

Zirconium, due to the nature and properties of its oxide, can be included in the so-called valve materials.[17] According to Dignam,[18] the two main characteristics of the oxidation behavior of these materials are: (*i*) the necessity of a high electric field to form an oxide film, *i.e.*, 10^6 V/cm or more and (*ii*) the formation of a film with a quasi-constant stoichiometry. Moreover, Patrito *et al.* define valve materials as materials in which the oxide blocks anodic electronic transfer reactions but not cathodic ones.[17]

Zirconium corresponds to these descriptions. Each estimation of the electric field in the film leads to values higher than 10^6 V/cm.[18-25] X-ray photoelectron spectroscopy (XPS) measurements indicate that, for all the values of pH studied, the stoichiometry of the thin oxide film is ZrO_2, even though a thin external hydroxide layer is also occasionally mentioned.[16] Moreover, Meisterjahn *et al.* indicate that anodic electronic transfer reactions are completely blocked while the cathodic ones can be achieved at potentials close or below the flatband potential.[16]

However, zirconium also exhibits features different from other valve materials. The oxide films are amorphous on Ta, Nb, or Al, while they are microcrystalline on zirconium. Diffraction patterns obtained by transmission electronic microscopy (TEM) indicate that zirconia is constituted of tetragonal and monoclinic phases.[9,23,24] Similarly, Ta, Nb, or Al have significant cationic transport numbers, while zirconium is characterized by a very low transport number for the metallic ions, t_m.[6,25,26] Thus, on films formed with current densities between 1 and 10 mA/cm^2, Davies *et al.*[25] found t_m values below 0.05. Khalil *et al.*[26] measured a t_m value of 0.22 in a solution of 0.1 *M* Na_2SO_4 and a current density of 50 mA/cm^2. This value is the highest one found in the literature.

The diffusion paths of oxygen in zirconium oxide films have also been studied. Whitton[6] deduced from his experiments that oxygen migration does not take place through the oxide bulk but through "easy" paths such as "defects, holes, crystallite boundaries, etc." It is generally accepted that the easiest paths for oxygen diffusion are grain boundaries.[4,6,27] Ortega and Siejka, however, using the results of tracers techniques, proposed a different mechanism: the oxygen would migrate in regions of higher ionic conductivity that were not necessarily limited to grain boundaries.[23]

Whatever the oxygen diffusion path may be, since oxygen ions are the only mobile ionic species, growth of the film takes place at the metal/oxide interface. The zirconium itself is a network former. The potential through the layer is the result of the distribution of these mobile anions and, according to Fehlner and Mott,[28] the film tends to grow under a constant field. Nevertheless, a few authors have measured electric fields in films with increasing thickness.[28-31] These observations were done by galvanostatic treatments with current densities equal or higher than 1 mA/cm^2. It is worth noting that the thickness dependence of the electric field has always been observed for high potentials (50 V).

Di Quarto *et al.*[31] explain such an increase by the presence of a mobile ionic space charge while Rogers *et al.*[29] correlate this phenomenon with the incorporation of species coming from the electrolyte.[32] Indeed, the incorporation of species such as sulfates, carbonates, or citrates decreases the oxygen vacancy concentration and consequently affects the ionic conductivity of zirconia and therefore the electric field. The extent of incorporation depends on the electrolyte but also on the formation current density and the pH of the solution. Incorporation may reach 0.1 SO_4^{2-} anions per molecule of ZrO_2. Leach and Pearson developed a model for the incorporation of anions coming from the solution.[33] According to this model, the quantity of incorporated anions depends on the ratio (anion)/(OH^-) at the external surface of the film. This criterion takes into consideration the influence of pH and of the imposed current density. Indeed, any variation of the applied current density may modify the local concentration of ions, particularly at the oxide/solution interface.

In other respects, the structure of anodic zirconium oxide films varies with the different electrolytes. Most of the time, the oxide is dense. This is the case in H_2SO_4, Na_2SO_4, and KOH. Sometimes, porous oxides are obtained in solutions containing nitrate, chromate, dichromate, or phosphate ions.[22,24,34]

The main features of thin zirconium oxide films are then: (*i*) growth in the presence of a high electric field, (*ii*) quasi-constant stoichiometry, (*iii*) a very low cationic transport number, and (*iv*) likely incorporation of species coming from the electrolyte.

In this work, we study oxidation of Zircaloy-4. The main difference between zirconium and Zircaloy-4 is the presence of intermetallic precipitates. Their surface fraction can be estimated to be about 1.5% with an average precipitate diameter of 200 nm (volumetric fraction for this alloy is 0.7%). These precipitates have been shown to undergo a delayed oxidation compared to the Zr matrix.[35] They constitute a short circuit for electronic conduction[36] and are associated to the occurrence of side reactions on the Zircaloys.[37] Thus, electronic leakage may occur through the precipitates. Nevertheless, Patrito *et al.*[37] showed that, below 2 V/SCE (saturated calomel electrode). Their behavior is the same as pure zirconium and that side reactions do not take place. This is no longer the case at higher potentials.

We have studied the electrochemical behavior of Zircaloy-4 through open-circuit potential (OCP) measurements for long times (48 h). We also perform potentiodynamic experiments as carried out by Meisterjahn *et al.*[16] and Patrito *et al.*[17] This leads to the determination of the high field law parameters: j_0 and F^*. Similar results to these have already been interpreted by Kirchheim[38] for other materials in terms of mobile defects. Thus, a specific experiment is performed to investigate the role of mobile defects in the oxidation of Zircaloy-4.

Experimental

Material.—Zircaloy-4 samples supplied by Cezus were used. They are described in Table I. From the initial sheet, 12 mm diam pellets were obtained. They were mechanically polished using SiC papers (1000, 2400, and 4000). They were then cleaned for 5 min with ultrasonic waves in a bath composed of 50% methanol and 50% acetone. A mirror surface was finally achieved by polishing with an OP-S solution from Struers (0.04 μm particles, pH 9.8). The samples were then cleaned once more (for 5 min with ultrasonic waves in a bath composed of 50% methanol and 50% acetone). The samples were exposed to air during a period of 24 h before the experiment.

Table I. Composition of the studied material.

Material	Weight composition (ppm)	
Zircaloy-4	Cr	1100
	Fe	2200
	O	1200
	Sn	14400

Electrochemical conditions.—The reference electrode was a saturated calomel electrode (SCE). The counterelectrode was a sheet of platinum (8 × 8 × 0.3 mm). The working electrode was the Zircaloy-4 sample. The surface in contact with the electrolyte was 0.237 cm^2.

The experiments were performed in a solution of 1 *M* Na_2SO_4 with pH of 6.6, which was adjusted just before the experiment. The solution was aerated.

The potentiostat was an EG&G Princeton Applied Research Corp. 263. The typical procedure for each experiment was to maintain the sample at the rest potential for 15 min before applying the desired conditions.

Different types of experiments were performed: (*i*) electrochemical anodic potentiodynamic sweeps from the OCP (after a delay of 15 min in the solution) to 2 V/SCE at increasing scan rates from 0.5 mV/min to 1 V/min. A potentiodynamic sweep was made by increasing the voltage every 250 μs (minimum time obtained for low scan rates). Successive anodic potentiodynamic sweeps were also performed (from the OCP to 1 V/SCE and then from 0 to 1 V/SCE). (*ii*) OCP studies (from 15 min to 2 days). (*iii*) OCP studies after a potentiodynamic sweep (the sweep was stopped at 1 V/SCE and the OCP was followed for 2 h).

Results

Evolution of the OCP.—Longtime experiments show that the evolution of the OCP exhibits two domains (see Fig. 1). Most of the time, the OCP varies linearly with time, at least for 48 h, with a slope of 0.05 mV/min. Nevertheless, during the first hours, the potential increases with time according to a law which could be logarithmic.

Anodic potentiodynamic sweeps.—The curves corresponding to each different scan rate are shown on Fig. 2. As expected, no activation peak was obtained. For each scan rate, a rapid increase of the anodic current density was measured, followed by a plateau as described by Patrito *et al.*[17] A plot of the values of the current density at 1 V/SCE (*i.e.*, on the plateau) for each scan rate can be fitted with a straight line (see Fig. 3) as

$$I = C(dV/dt) \quad [1]$$

where C has a dimension of a capacity per area unit. Its value is found to be approximatly 15 mF/cm^2.

The plateau ends at a potential, E_c, dependent on the scan rate according to a logarithmic law with a slope of approximately 90 mV/dec (see Fig. 4). This point, possibly related to the oxygen evolution reaction, is not discussed in this paper.

Repetitions of sweeps done on the same specimen immediately after each other lead to results completely different to those observed on the first scan (see Fig. 5). The measured current density appears to depend almost exponentially on the imposed potential. Moreover, at 0.2 V/SCE,

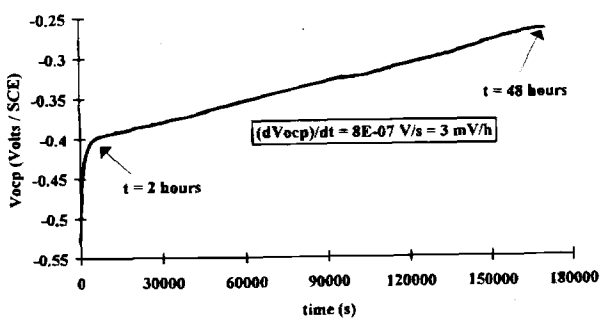

Fig. 1. Evolution of the OCP for 2 days.

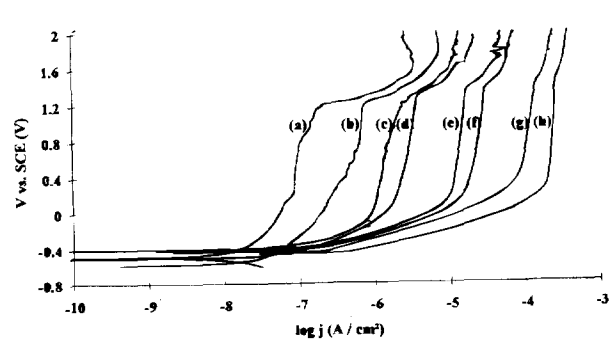

Fig. 2. Potentiodynamic curves obtained at different scan rates: (a) 0.5, (b) 2, (c) 5, (d) 10, (e) 50, (f) 100, (g) 500, and (h) 1000 mV min^{-1}.

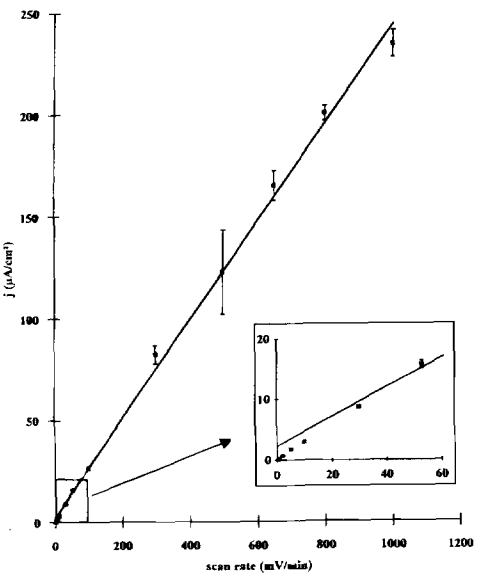

Fig. 3. Evolution of the current density at 1 V/SCE *vs.* scan rate. The inset shows detail of the results at low scan rate.

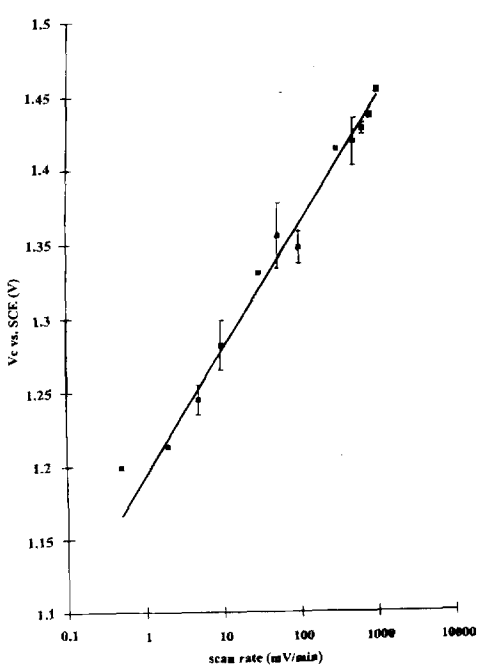

Fig. 4. Evolution of the end of the plateau, V_c, *vs.* scan rate.

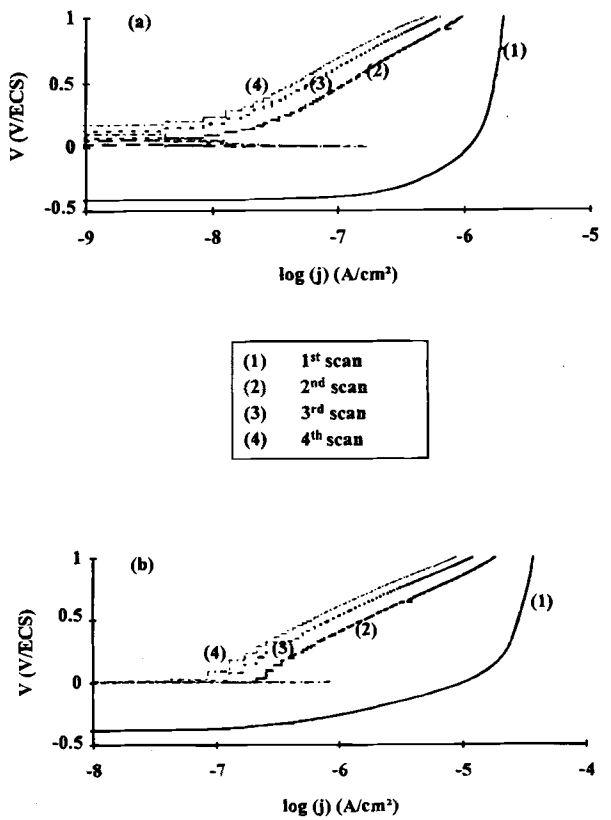

Fig. 5. Sequential potentiodynamic sweeps at (a) 5 and (b) 100 mV min^{-1}.

the current density during the second sweep is two orders of magnitude lower than during the first one. At 1 V/SCE, it is only two times lower. During the third and fourth scans, the current density is still decreasing and continues to follow the same dependence *vs.* the imposed potential. These experiments have been performed at different scan rates (5, 100, and 1000 mV/min). The behavior was always the same.

We have also observed for the lowest scan rate (0.5 mV/min) that, even if the sweep is performed in the anodic direction, there is a cathodic net current at the beginning (see Fig. 2, curve a). Moreover, if the delay at the OCP is decreased, this cathodic net current density is observed up to higher scan rates. On Fig. 6, the sample was left for 100 s at the OCP before the beginning of a potentiodynamic sweep at 3 mV/min. A cathodic current is observed during 500 s before becoming anodic, while it is always anodic when the sweep begins after 15 min at the OCP for scan rates higher than 0.5 mV/min (see Fig. 2).

Evolution of the OCP after a potentiodynamic sweep.—The aim of this experiment is to study the return to equilibrium of the oxide film after different growth conditions. Thus, potentiodynamic sweeps at increasing scan rates are performed up to V_1 = 1 V/SCE and then interrupted. The evolution of the OCP is then recorded. A typical curve is presented in Fig. 7.

In each case, as soon as the sweep is interrupted, we measure a sharp decrease of the OCP. The amplitude, $(V_1 - V_{min})/(V_1 - V_{t0})$, and rapidity, $t_{min} - t_1$, of the decrease appear to depend on the previously imposed scan rate (see Fig. 8a and b). After a low scan rate (*e.g.*, 1 mV/min) the OCP decreases for more than 2 h. After a scan rate of 1 V/min, the OCP reaches its minimum value, V_{min}, after 3 min. Thus, the higher the scan rate, the shorter the decrease of the OCP.

Another observation concerns V_{min}. For low scan rates, this minimum OCP is higher than the OCP measured just before the potentiodynamic sweep. On the contrary, for

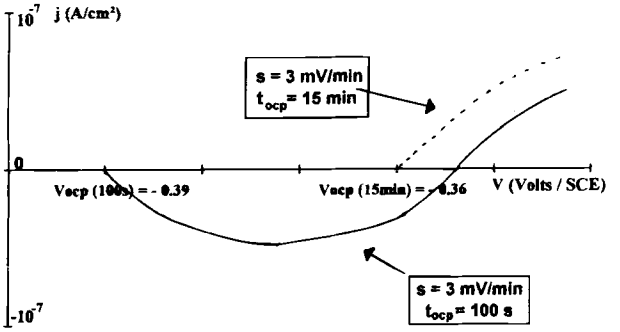

Fig. 6. Beginning of potentiodynamic sweeps in the anodic direction for a scan rate of 3 mV min^{-1} after two delay times at the OCP: 100 s and 15 min. For the first delay time, the scan rate is lower than the rate of variation of the OCP (16 mV min^{-1}). The current is then cathodic for 26 mV. On the other hand, after 15 min at the OCP, the scan rate is larger than the rate of variation of the OCP; no cathodic current is observed.

high scan rates (>100 mV/min), the minimum OCP, V_{min}, reaches values below those measured before the sweep. This point is not discussed.

Data Analysis

Rest potential.—The measured OCP can be decomposed into three terms

$$V_{ocp} = V_H + V_{ext} + V_f \quad [2]$$

with V_H being the difference of potential through the Helmoltz double layer, V_{ext} the difference of potential in the other parts of the circuit, V_f the difference of potential through the film equal to FL, F the electric field in the film, and L the film thickness.

Assuming that the potential is constant across the interfaces, it becomes

$$dV_{ocp}/dt = d(FL)/dt \quad [3]$$

According to many authors, zirconium alloys grow under a high-field-type mechanism.[17,40] Bacarella and Sutton[41] consider that this is only true for temperatures below 170°C, which is the case in our experiments. With this mechanism, the growth of the film can be written as

$$dL/dt = K \exp(BF) \quad [4]$$

where K is the kinetic constant, $B = \alpha Zq\delta/kT$;[38] k is the Boltzman constant; T is temperature (293 K); α is the symmetry factor taken between 0 and 1 to describe the activation barrier for a jump (in the present analysis we assume a reasonable value of α, *i.e.*, 0.5); Z the charge of the mobile species with a value of -2 since oxygen is the

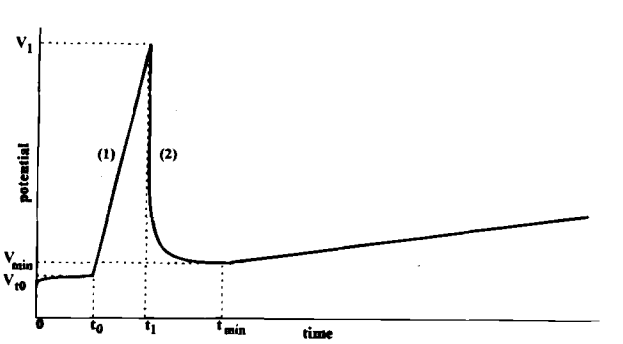

Fig. 7. Schematic representation of an experiment consisting of (1) a potentiodynamic sweep followed by (2) a record of the OCP. t_0 is the time at the beginning of the sweep, t_1 at the end, and t_{min} the time for the OCP to reach its minimum value.

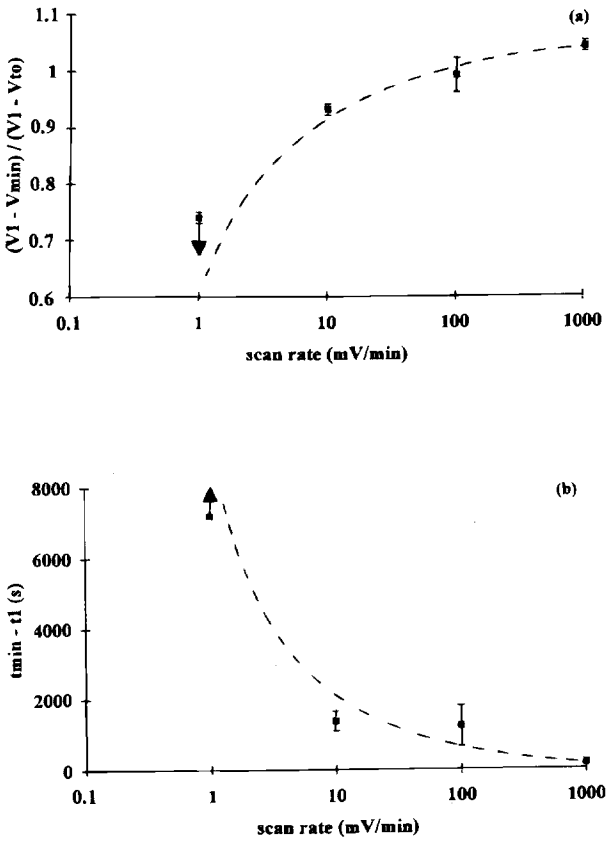

Fig. 8. Influence of the scan rate on the OCP evolution after a potentiodynamic sweep: (a) evolution of the ratio $(1 - V_{min})/(1 - V_{t0})$ and (b) evolution of the time necessary to reach V_{min} after the sweep. Note: at 1 mV min^{-1}, the OCP was still decreasing after 2 h.

mobile species; q the charge of an electron; and $\delta = 2.7$ Å (mean value between two O atoms in monoclinic ZrO_2.[39] This leads to

$$1/B = F^* = 6.2 \times 10^5 \text{ V/cm}$$

where F^* is referred to as the characteristic field for film growth to operate following the high-field mechanism.

Assuming that for our experimental conditions the electric field is constant in the film, Eq. 3 and 4 imply that dV_{ocp}/dt is constant. This result should be obtained if there is only film growth under a constant high electric field. This is only the case after a long delay time. We are also aware that such a result may be due to other phenomena than film growth, but it is consistent with film growth. At the begining of the OCP evolution (see Fig. 9), even if the values are not always reproducible and appear to depend on the initial surface features, V_{ocp} follows a logarithmic law described by Eq. 5

$$V_{ocp} = V_0 + A \ln (1 + t/\tau) \quad [5]$$

where V_0 is the potential at $t = 0$, t is the time, and A and τ are constants.

During this period, we can then assume that one of the two previous hypotheses is no longer valid. Thus, V_H and/or F probably vary in order to attain the steady-state values encountered in the linear domain.

Potentiodynamic experiments.—The value of the capacity obtained by plotting the current density at 1 V/SCE *vs.* the scan rate is too high to be linked with the capacity of the Helmoltz double layer. Indeed, in our solution, due to the low concentration of our electrolyte, we can consider the diffuse layer as one molecular layer. In this case, the Helmoltz double layer is a few angstroms thick and its capacity is estimated to be a few tens of μF/cm^2.[42]

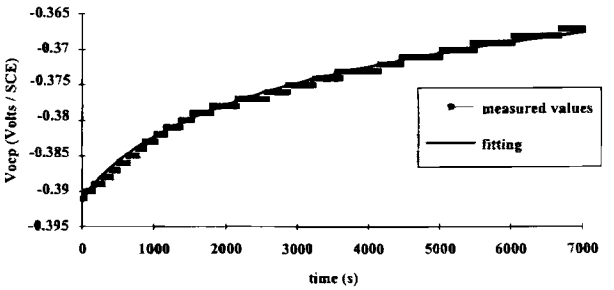

Fig. 9. Fitting of the beginning of the OCP evolution by a logarithmic law: $V = V_0 + A \ln (1 + t/\tau)$, where $V_0 = -0.391$ V, $A = 0.098$, and $\tau = 700$ s.

Moreover, since the oxide film is much thicker, its capacity is much lower (a few μF/cm^2).

Keddam *et al.* observed the same phenomenon on stainless steel.[43] They noted that the C value obtained was half the value expected for the anodic formation of a ferric oxide layer, assuming a 30 nm/V thickness potential dependence. Similarly, we have checked that our C value was compatible with the values of electric field classically measured in zirconium oxide layers.

The necessary electric charge per unit area, $d\sigma$, to build an oxide layer of thickness dL, is

$$d\sigma = \nu dL \quad [6]$$

with $\nu = (qz/\delta^3) = 18480$ C/cm^3 and $z = 4$ (charge of the Zr cation).

Assuming a constant electric field throughout the film

$$FdL = dV_f \quad [7]$$

leading to a film growth-induced capacity

$$C = d\sigma/dV_f = \nu/F \quad [8]$$

The results shown in Fig. 3 suggest that $C = 15$ mF/cm^2 whatever the scan rate, which leads to an electric field $F = 1.3\ 10^6$ V/cm, whose order of magnitude is typical of the electric field found in oxide layers. For instance, the same calculation with the results of Brown *et al.*[19] on Zr and Zircaloy-2 in 0.1 *M* NaOH yields a value of $F = 3 \times 10^6$ V/cm. The plateau observed on our *I-V* curves can then be directly related to the growth of the oxide film. Nevertheless, more detailed analysis shows that F slightly depends on the scan rate (see below), ranging from 1.1×10^6 V/cm for $s = 0.5$ mV/min to 1.5×10^6 V/cm for $s = 1$ V/min leading to 1.3×10^6 V/cm as an average value.

The preceding point indicates that the measured currents are in accordance with an oxide growth under a constant high-field mechanism and are thus consistent with the hypothesis of a minor role of the intermetallics at the potentials explored. Repetitions of sweeps give a clue as to the possible amount of electronic leakage through these intermetallics.

Should the electronic leakage significantly contribute to the plateau current, this current value would be nearly the same for the first and the second sweep. It is clearly not the case, at least for low enough potentials (typically from +0.2 to +0.6 V/SCE where the current for the second sweep is one or two orders of magnitude smaller than for the first sweep). Thus, the polarization curves obtained for the first sweep mainly correspond to passive film growth.

For the subsequent sweeps, we feel that electronic leakage contributes significantly to the measured current. This current slightly decreases with the number of sweeps possibly due to a precipitate passivation.

These results are consistent with those of Patrito *et al.*[37] who do not find any evidence of side reactions at the intermetallics below 2 V/SCE. Moreover, in nitric solutions, after dissolution of the intermetallics the current density goes back to the value of the plateau and remains constant.

Thus, the hypothesis of a minor role of the precipitates in the present electrochemical approach appears to be reasonable and in the following discussion the current on the plateau will be considered as a film growth current.

At the beginning of the sweep, the current density is probably due not only to the growth of the film. In fact, it appears to be correlated to the evolution rate of the OCP, dV_{ocp}/dt, just before the potentiodynamic sweep. Indeed, $(dV_{ocp}/dt)_{15min}$ is around 0.9 mV/min. We observed a cathodic net current density only when the scan rate is lower than the former value. On another hand, $(dV_{ocp}/dt)_{100s}$ is determined to be 16 mV/min and a sweep after 100 s at 3 mV/min results in a cathodic current density for 500 s. As $(dV_{ocp}/dt)_{15min} < 3$ mV/min $< (dV_{ocp}/dt)_{100s}$, the threshold scan rate for which a cathodic net current density is observed depends clearly on the evolution rate of the OCP and, consequently, on the exposure time just before the potentiodynamic sweep.

Discussion

Potentiodynamic experiments.—During a potentiodynamic experiment, a potential, V, is applied across the film. This potential can also be separated into three terms as in Eq. 2. By differentiating Eq. 2, and assuming that V_{ext} is constant (as it results from the ohmic drop in the solution and from the potentials at the other interfaces than those of the oxide film), we obtain the scan rate, s

$$s = dV/dt = dV_f/dt + dV_H/dt \quad [9]$$

We observe a plateau on the I-V curves. Even if the current density is not absolutely constant on this plateau, it varies very slowly (not less than 3 V/dec). This plateau can be analyzed as a quasi-steady-state event where the electric field remains constant and leads to a growth of the oxide film. The double layer may be assumed to be at equilibrium ($dV_H/dt = 0$). Thus

$$dL/dt = j_s/\nu \quad [10]$$

with j_s the growth current density. Since $V_f = FL$ (see Eq. 2), Eq. 9 can be written

$$s = LdF/dt + FdL/dt \quad [11]$$

Combining Eq. 10 and 11 yields

$$s = (V_f/F)sdF/dV + Fj_s/\nu \quad [12]$$

$$dF/dV = [1 - Fj_s/(\nu s)]F/V_f = 0 \quad [13]$$

Finally, we obtain

$$\nu s/j_s = F = F^* \ln (j_s/j_0) \quad [14]$$

where s and j_s are known experimentally. The plot of the function $\nu s/j_s = f[\ln (j_s)]$ (Fig. 10) should lead to a straight line giving the values of the characteristic field F^* [slope of $\nu s/j_s$ *vs.* $\ln (j_s)$] and of j_0: $F^* = 0.9 \times 10^5$ V/cm and $j_0 = 7 \times 10^{-10}$ A/cm^2.

This F^* value is smaller than that previously calculated from Eq. 4 ($F_c^* \sim 6 \times 10^5$ V/cm). Such a difference was already explained by Kirchheim[38]: when changing the current density, j, through a passive film (which is the case when the scan rate is changed), the system can react in two ways: either by changing the electric field throughout the film and/or by changing the concentration of moving defects. These two phenomena are taken into account in the following expression

$$d \ln j = k \ln c + 1/F_c^* dF \quad [15]$$

with c being the concentration of moving defects and k the proportionality constant.

To calculate F^* with our experimental values, we have neglected any changes in the concentration of moving defects and used

$$d \ln j_s = 1/F^* dF \quad [16]$$

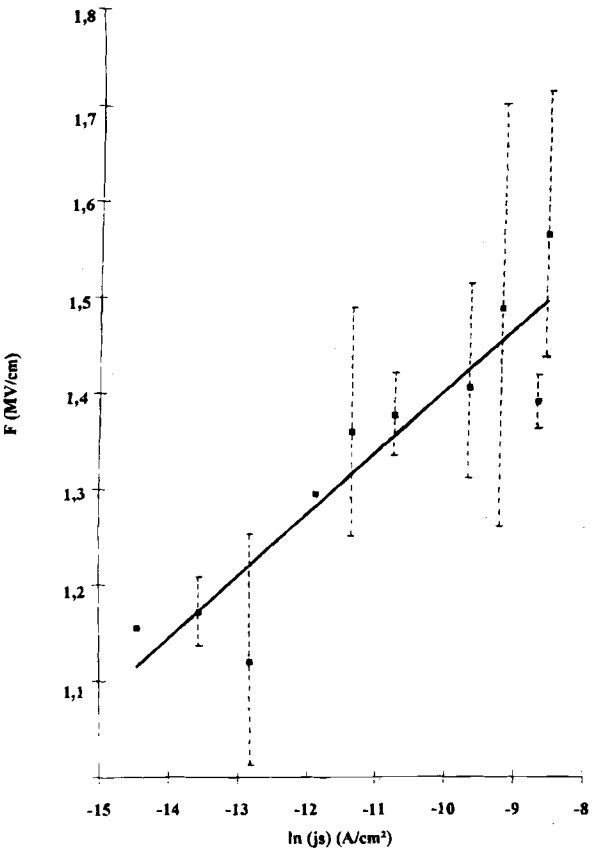

Fig. 10. Determination of the characteristic field F^* and j_0 according to Eq. 13.

By comparing Eq. 14 and 15, Kirchheim concludes that any measurements of the current density or the potential, using this approach, yield a value of F^* which is smaller than F_c^*, if the defect concentration increases with increasing current density. Moreover, similar discrepancies were obtained by Ortega with zirconium in citrate solutions.[23] Indeed, he found values of F^* varying from 1.1 to 1.4 $\times$ 10^5 V/cm, depending on the temperature (from 0 to 60°C), without explaining the differences with the theoretical values; however, he mentioned similar tendencies in various glasses.

The evolution of defect concentration with scan rate could also be an explanation of the observed increase of F. In this case, F would remain constant whatever the scan rate with a value which can be obtained by calculating the slope of $I = CdV/dt$ (Fig. 3) for $dV/dt = 0$. That leads to $C_{dV/dt(0)} = 22$ mF/cm^2 and thus to a value for the electric field of 0.9×10^6 V/cm. That is the electric field that must be present in the film under the open-circuit conditions. Using the measured evolution rate of the OCP, *i.e.*, 0.05 mV/min, and Eq. 13, we obtain $j = 16$ nA/cm^2. As $j_0 = j/\exp(F/F^*)$, it leads to $j_0 = 5$ nA/cm^2.

In conclusion, the results of our potentiodynamic experiments are in good agreement with the assumption of a constant high field mechanism. Nevertheless, it could be interesting to take into account in the modeling, the presence of defects at the film surface as in the bulk, since the difference between F^* and F_c^* tends to indicate that the concentration of moving defects in the film is high, as already mentioned by Chao *et al.*[44]

OCP after potentiodynamic sweep.—The OCP evolution after a potentiodynamic sweep up to 1 V/SCE appears to depend on the scan rate. After a rapid sweep, we measure a large and fast decrease of the OCP, while after a slow sweep, the OCP decrease is moderate. This results in an increase of the ratio $(V_1 - V_{min})/(V_1 - V_{t0})$ and a decrease of $(t_{min} - t_1)$ as the scan rate increases (see Fig. 7a and b).

Such a behavior can be tentatively analyzed in terms of the concentration of mobile defects[38] (see Fig. 11a and b). At t_0, when the potentiodynamic sweep begins, the electric field in the film is F_0 and the concentration of mobile defects is c_0. At t_1, just before the end of the sweep, the electric field F_1 can be written as

$$F_1 = V_{f1}/(L_0 + \Delta L) \quad [17]$$

with V_{f1} being the value of the difference of potential through the film when V_{ap} = 1 V and ΔL the film thickening during a sweep that is supposed to be independent of scan rate.

During the potential sweep, the concentration of mobile defects is increased from its initial value c_0 to c_1. Just after t_1, when the sweep is interrupted, the film goes back under open-circuit conditions and the same equation as Eq. 17 gives the value of the electric field, $F_{ocp}(t_1)$, just after the interruption

$$F_{ocp}(t_1) = V_f(\text{ocp})/(L_0 + \Delta L) \quad [18]$$

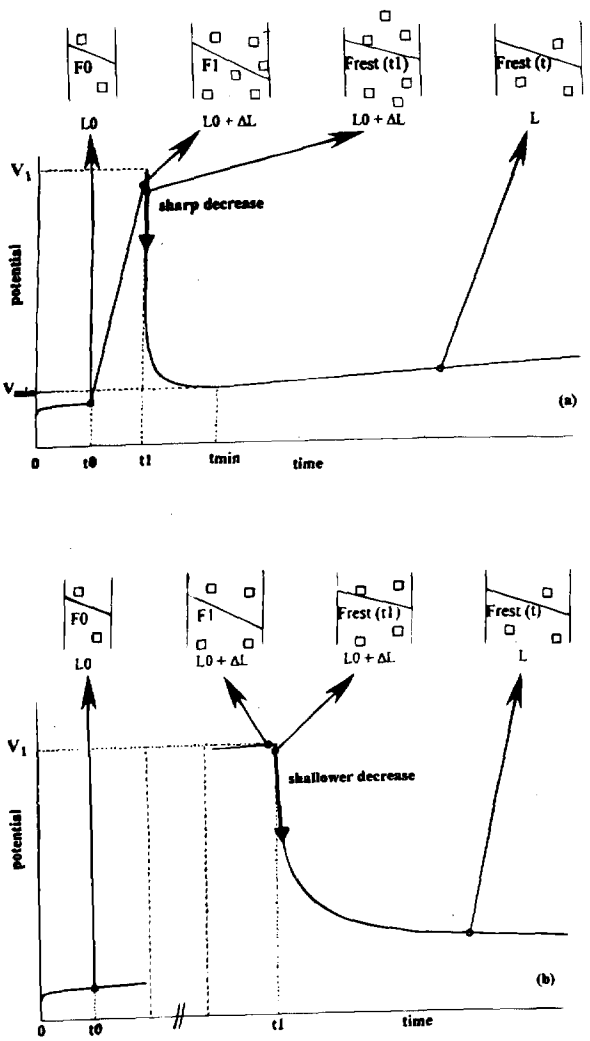

Fig. 11. Concentration of mobile defects and electric field within the film for different times: ($t < t_0$) is growth of the film at OCP under constant electric field; ($t_0 < t < t_1$) the potentiodynamic scan; on the plateau the electric field and the concentration of mobile defects increase; ($t = t_1$) the end of the scan; ($t \geq t_1$) the concentration of mobile defects is larger than before $t = t_0 \Rightarrow F_{rest}(t_1)$ is smaller than F_0; ($t >> t_1$) the mobile defects are annihilated at the interface oxide/solution and the growth continues on. The electric field increases from $F_{rest}(t_1)$ to a new value $F_{rest}(t)$; (a) is the high scan rate and (b) the slow scan rate.

with V_f(ocp) the value of the difference of potential through the film under open-circuit conditions.

Since the film is under open-circuit conditions we can assume that the current density corresponding to film growth is constant. In these conditions, according to Eq. 14, any variation of the moving defect concentration is counterbalanced by a variation of the electric field within the oxide film. Thus, the higher the value of moving defect concentration, the smaller the electric field in the film, and consequently, the lower the measured value of V_f(ocp).

As soon as the sweep is interrupted, the concentration of moving defects, c_1, is significantly higher than c_0, resulting in a low value of $F_{ocp}(t_1)$. Then, moving defects tend to annihilate at the film-solution interface and the progressive decrease of their concentration leads to a subsequent increase of the electric field in the film. The combination of both phenomena, the film growth and the defect annihilation, gives a satisfactory explanation to the shape of the OCP measurements (see Fig. 11a and b).

According to Kirchheim, since c_1 is directly correlated to the current density through the oxide layer, it is reasonable to think that c_1 will increase with the scan rate. Thus, with a high scan rate, the value of $F_{ocp}(t_1)$ is expected to be relatively low and the sudden potential decrease more pronounced. At the same time, as the concentration of moving defects is high, the annihilation process is more efficient. The resulting experimental curve is presented on Fig. 11a for s = 100 mV/min. The OCP decrease is sharp but ends rapidly. On Fig. 11b (for s = 1 mV/min), c_1 is expected to be close to c_0 since at t_0 the imposed scan rate was not very different from the growth rate of the film under rest conditions. Then, the potential decrease is observed to be quite soft and is due to the slow annihilation with low concentration of moving defects; the stabilization of the OCP occurs after a long time.

Thus, our results can be interpreted in terms of a concentration evolution of mobile defects in the oxide layer.

It is worth noting that these results are of the same nature as the overshooting effects reported by Adams *et al.*[45] who studied the electrical behavior of zirconium below the oxygen evolution potential using aqueous solutions of ammonium borate and sodium carbonate. They noted that when the current applied to the zirconium electrode is abruptly raised, the potential overshoots its final value before returning to steady growth conditions. Similar results on niobium are interpreted by Young as an evidence of ionic space charge which would take some time to readjust as the current density was rapidly changed.[30] Vetter[46] notes that concentration of defects may play a role in the overshooting effects while Willis *et al.*[47] remarks that this effect could also be explained in terms of a lag in the increase of the surface concentration of active sites from lower to higher steady values.

Finally, the preceding discussion tends to indicate that the incorporation of extrinsic anions is a second-order effect. Indeed, according to Leach and Pearson,[33] the higher the scan rate, the higher the incorporation of anions coming from the electrolyte (SO_4^{2-} ions in our case). Such an effect should result in a decrease of the concentration of mobile defects with increasing scan rates which is in contrast to our results.

Conclusions

The OCP (V_{ocp}) time dependence (up to 48 h) is found to provide relevant, although aggregate, information on passive film evolution when Zircaloy is immersed in the test solution. For short exposure time (~2 h), a logarithmic time dependence is apparent, possibly corresponding to the onset of stationary behavior. For longer exposure times (2 h to 2 days), V_{ocp} increases linearly with time, which could be due to the film growth under a constant high electric field (evaluated to be of the order of 10^6 V/cm).

Potentiodynamic experiments with different scan rates (s) provide further information confirming high-field passive film growth, with an electric field varying from 1.1 × 10^6 V/cm for s = 0.5 mV/min to 1.5 × 10^6 V/cm for s =

1 V/min. These experiments also allow determination of a characteristic field, F^* for the high-field mechanism (growth rate proportional to exp $[F/F^*]$). The value of F^* is found to be 0.9×10^5 V/cm. A theoretical assessment of F^* leads to $F^* = 6.2 \times 10^5$ V/cm.

The difference between the theoretical and experimental values for the characteristic field is explained by the effect of the concentration of mobile defects, c, contributing to the film growth, as previously suggested by Kirchheim. Further modeling is proposed, taking into account the effect of c on the apparent electric field deduced from the potentiodynamic tests. The true electric field through the film, F_0, is assumed to be independent of s and is obtained from the limit of $F(s)$ at $s = 0$. It was found that $F_0 \sim 10^6$ V/cm.

The proposed model also predicts that the mobile defect concentration increases with scan rate. Measuring the OCP decay after a potentiodynamic scan up to 1 V/SCE shows that the decay becomes larger and faster when s increases, which is consistent with relaxation of the mobile defects concentration.

Acknowledgments

We gratefully acknowledge the assistance of B. Cox and C. Lemaignan for their fruitful and stimulating discussions.

Manuscript submitted Aug. 22, 1995; revised manuscript received Aug. 20, 1996.

C.E.A. Grenoble DTP/SESS assisted in meeting the publication costs of this article.

REFERENCES

1. A. A. Strasser and M. G. Andrews, in *Proceedings of IAEA Technical Committe Meeting on Fundamental Aspects of Corrosion of Zirconium Base Alloys in Water Reactor Environments*, Portland, Sept. 1989, IAEA IWGFPT\34 ISSN 1011-2766 (1990).
2. F. Garzarolli and H. Stehle, in *Proceedings of IAEA Int. Symposium on Improvements in Water Reactor Technology and Utilization*, Stockholm, Sept. 1986, IAEA SM-288-24 (1987).
3. F. Garzarolli, E. Steinberg, and H. G. Weidinger, *ASTM-STP*, **1023**, 202 (1989).
4. C. M. Eucken, P. T. Finden, S. Trapp-Pritsching, and H. G. Weidinger, *ibid.*, **1023**, 113 (1989).
5. J. Godlewski, J. P. Gros, M. Lambertin, J. F. Wadier, and H. G. Weidinger, *ibid.*, **1132**, 416 (1991).
6. J. L. Whitton, *This Journal*, **115**, 59 (1968).
7. J. A. Davies, B. Domeij, J. P. S. Pringle, and F. Brown, *ibid.*, **112**, 675 (1965).
8. J. S. Bryner, *J. Nucl. Mater.*, **82**, 84 (1979).
9. X. Iltis, B. Stauder, H. Michel, and C. Frantz, *Surf. Coating Techn.*, **60**, 405 (1993).
10. B. Cox and J. P. Pemsler, *J. Nucl. Mater.*, **28**, 73 (1968).
11. B. Wadman, H. O. Andrén, A. L. Nyström, P. Rudling, and H. Pettersson, *ibid.*, **200**, 207 (1993).
12. C. Lemaignan, *ibid.*, **187**, 122 (1992).
13. D. Gorse and T. Sakout, *Solid State Phenom.*, **30-31**, 451 (1993).
14. G. Mankowski, C. Lemaître, and H. H. Strehblow, in *Corrosion Localisée*, F. Dabosi, G. Beranger, and B. Baroux, Editors, p. 173, Les Editions de Physique, Les Ulis, France (1994).
15. S. Preusser, U. Stimming, and K. Wippermann, *Electrochim. Acta*, **39**, 1273 (1994).
16. P. Meisterjahn, H. W. Hoppe, and J. W. Schultze, *J. Electroanal. Chem.*, **217**, 159 (1987).
17. E. M. Patrito, R. M. Torresi, E. P. M. Leiva, and V. A. Macagno, *This Journal*, **137**, 524 (1990).
18. M. J. Dignam, in *Oxides and Oxide Films*, Vol. 1, J. W. Diggle, Editor, p. 91, Marcel Dekker, Inc., New York (1972).
19. M. A. Hopper, J. A. Wright, and D. J. Smet, *This Journal*, **124**, 44 (1977).
20. M. L. Brown and G. N. Walton, *J. Nucl. Mater.*, **58**, 321 (1975).
21. M. L. Brown and G. N. Walton, *ibid.*, **66**, 44 (1977).
22. R. A. Ploc and M. A. Miller, *ibid.*, **64**, 71 (1977).
23. C. Ortega and J. Siejka, *This Journal*, **129**, 1895 (1982).
24. B. Cox, *ibid.*, **117**, 654 (1970).
25. J. A. Davies, B. Domeij, J. P. S. Pringle, and F. Brown, *ibid.*, **112**, 675 (1965).
26. N. Khalil, A. Bowen, and J. S. L. Leach, *Electrochim. Acta*, **33**, 1721 (1988).
27. B. Cox and C. Roy, *Electrochem. Technol.*, **4**, 121 (1966).
28. F. P. Fehlner and N. F. Mott, *Oxid. Met.*, **2**, 1 (1970).
29. G. T. Rogers, P. H. G. Draper, and S. S. Wood, *Electrochim. Acta*, **13**, 251 (1968).
30. L. Young, *Trans. Faraday Soc.*, **55**, 632 (1959).
31. F. Di Quarto, S. Piazza, and C. Sunseri, *ibid.*, **130**, 1014 (1983).
32. J. C. Banter, *ibid.*, **114**, 508 (1967).
33. J. S. L. Leach and B. R. Pearson, *Electrochim. Acta*, **29**, 1263 (1984).
34. B. Cox, F. Gascoin, and Y. M. Wong, *J. Nucl. Mater.*, **218**, 113 (1995).
35. D. Pêcheur, F. Lefebvre, A. T. Motta, C. Lemaignan, and J. F. Wadier, *ibid.*, **189**, 318 (1992).
36. B. Cox, in *Advances in Corrosion Science and Technology*, Vol. 5, p. 173, R. E. Fontana and R. W. Staehle, Editors, p. 173, Plenum, New York (1976).
37. E. M. Patrito, R. M. Torresi, E. P. M. Leiva, and V. A. Macagno, *Electrochim. Acta*, **37**, 281 (1992).
38. R. Kirchheim, *Corros. Sci.*, **29**, 183 (1989).
39. D. K. Smith and H. W. Newkirk, *Acta Crystallogr.*, **18**, 983 (1965).
40. P. Meisterjahn, U. König, and J. W. Schultze, *Electrochim. Acta*, **34**, 551 (1989).
41. A. L. Bacarella and A. L. Sutton, *Electrochem. Technol.*, **4**, 117 (1966).
42. B. Baroux and D. Gorse, in *Corrosion Localisée*, F. Dabosi, G. Beranger, and B. Baroux, Editors, p. 91, Les Editions de Physique, Les Ulis, France (1994).
43. M. Keddam, M. Krarti, and C. Pallotta, *Corrosion*, **43**, 454 (1987).
44. C. Y. Chao, L. F. Lin, and D. D. Macdonald, *This Journal*, **128**, 1187 (1981).
45. G. B. Adams, M. Maraghini, and P. Van Rysselberghe, *ibid.*, **102**, 502 (1955).
46. K. J. Vetter, *Electrochim. Acta*, **16**, 1923 (1971).
47. G. C. Willis, G. B. Adams, and P. Van Rysselberghe, *ibid.*, **9**, 93 (1964).